Battle the Wind: Improving Flight Stability of a Flapping Wing Micro Air Vehicle Under Wind Disturbance With Onboard Thermistor-Based Airflow Sensing

Wang, S.; Olejnik, D.A.; de Wagter, C.; van Oudheusden, B.W.; de Croon, G.C.H.E.; Hamaza, S.

DOI
10.1109/LRA.2022.3190609

Publication date
2022

Document Version
Final published version

Published in
IEEE Robotics and Automation Letters

Battle the Wind: Improving Flight Stability of a Flapping Wing Micro Air Vehicle Under Wind Disturbance With Onboard Thermistor-Based Airflow Sensing

Sunyi Wang, *Graduate Student Member, IEEE*, Diana Olejnik, Christophe de Wagter, Bas van Oudheusden, Guido de Croon, *Member, IEEE*, and Salua Hamaza, *Graduate Student Member, IEEE*

***Abstract*—Flyers in nature equip different airflow sensing mechanisms to navigate through wind disturbances with remarkable flight stability. Embracing bio-inspiration, airflow sensing with conventional sensors has long been utilized in flight control for larger micro air vehicles (MAVs). Bio-inspired flapping wing MAVs (FWMAVs) have extremely limited power and payload, therefore implementing onboard airflow sensing has remained a challenge in spite of various attempts at miniaturized airflow sensor designs. This work characterizes the measurement performance of a lightweight off-the-shelf thermistor-based airflow sensor through comparison with a hot-wire probe. Wind tunnel tethered flight tests on a 31.3-gram FWMAV Delfly Nimble examine the onboard sensing performance at low flow speeds (up to 2 m/s), under the influence of flapping motion. This performance characterization further motivates a miniaturized re-design of the airflow sensor with over 40% size and weight reduction. The redesigned airflow sensor helps to realize the first flapping wing MAV free flight with onboard airspeed measurements, providing remarkable flight stability under wind speeds in the range of approximately 0.5 to 1.2 m/s. This embodied sensing configuration pushes the weight and power limit of miniaturized electronics for FWMAVs, providing an easy-to-integrate solution with good performance, and paving the way for more complex control of FWMAVs in dynamic conditions.**

***Index Terms*—Biologically-inspired robots, Sensor-based control, Flapping wing, Thermal anemometer, Wind disturbance.**

I. Introduction

FLAPPING wings micro air vehicles (FWMAVs) are more susceptible to wind disturbances than other MAVs due to their lower wing loading. When flying in gusts, airflow sensing is often exploited on larger aerial platforms, e.g. fixed wing MAVs, to improve flight control and therefore performance. Traditional airflow sensing instrumentation such as a pitot tube cannot be as easily implemented on lightweight FWMAVs due to their larger size and mass. At lower flow speed regimes where FWMAVs can still operate under the disturbance, the small dynamic pressure changes would require larger transducers with higher sensitivity and hence scale up the instrumentation size quickly [1]. Bio-inspiration comes to the aid when it comes to fabricating lightweight novel airflow sensors, by mimicking the sensory receptors found in insects and birds [2]–[4].

Numerous attempts have been made to realize an engineering prototype of a bio-inspired hair-like airflow sensor that can sense airflow with sufficient accuracy, sensitivity and directionality [1], [5]–[10]. With a compact readout circuit, the airflow information can be acquired through measuring the resistance or capacitance change of a micro-cantilever structure caused by different amount of airflow induced vibrations and deflections. Prototypes such as a thin piezoresistive cantilever on a flapping wing made by Takahashi *et al.* [5] or a contact-resistance-based airflow sensor on a small quadrotor by Gollob *et al.* [7] have further indicated effective airflow sensing instrumentation has the potential to open up new applications for lightweight MAVs with limited payload, such as flow distribution analysis onboard the MAV in flight to aid flight stability.

However, due to the payload and power restriction, providing the bio-inspired airflow sensor with an effective readout and considering system level integration at a suitable placement location to a FWMAV still remains an unexplored area. Measurement noise arisen from flow boundary layer effects, inertial and aerodynamic force due to flapping motion, temperature fluctuations require tremendous effort to design, calibrate and characterize the sensor sufficiently before the inputs can be integrated to disturbance estimation and rejection scheme design.

Although an integrated solution with airflow sensing and processing onboard a FWMAV has not yet been available, attempts have been made to utilize airflow information to improve the flight stability under wind disturbance for different MAV platforms. Keshavan et Humbert [11] first proposed a theoretical sensing framework to augment the stability of a micro helicopter using hair-like sensors, and later Ranganathan *et al.* [12] realized

Manuscript received 24 February 2022; accepted 28 June 2022. Date of publication 13 July 2022; date of current version 26 July 2022. This letter was recommended for publication by Associate Editor Amir Shapiro and Editor Hyungpil Moon upon evaluation of the reviewers' comments. This paper was recommended for publication by Editor Hyungpil Moon upon evaluation of the Associate Editor and Reviewers' comments. This work was supported by Delft University of Technology. *(Corresponding author: Sunyi Wang.)*

Sunyi Wang, Diana Olejnik, Christophe de Wagter, Guido de Croon, and Salua Hamaza are with the Department of Control & Operations, Delft University of Technology, 2628 Delft, AX, Netherlands (e-mail: s.wang-12@tudelft.nl; d.a.olejnik@tudelft.nl; c.dewagter@tudelft.nl; guido.de.croon@gmail.com; s.hamaza@tudelft.nl).

Bas van Oudheusden is with the Department of Aerodynamics, Delft University of Technology, 2628 Delft, AX, Netherlands (e-mail: B.W.vanOudheusden@tudelft.nl).

Digital Object Identifier 10.1109/LRA.2022.3190609

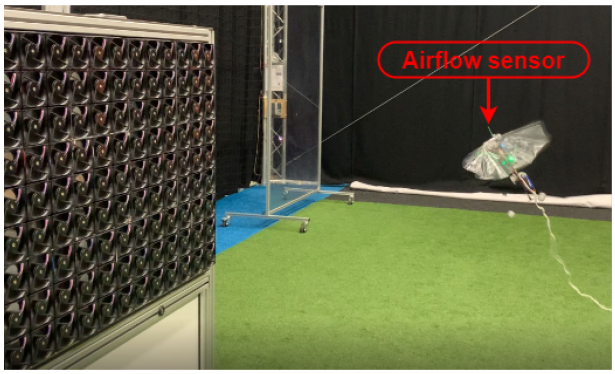

Fig. 1. The FWMAV Delfly Nimble with a thermistor-based airflow sensor onboard, performing a free flight under wind disturbance generated by a multi-fan system.

the sensor prototype with integrated signal readout circuitry to be used onboard a MAV to aid state estimation. Chiraratananon *et al.* [13] demonstrated that partial knowledge of wind speed and direction from external sources helps implement a disturbance rejection scheme that gives smaller position control error onboard a FWMAV. Lee *et al.* [14] modelled a FWMAV's attitude dynamics under wind disturbance and designed an attitude controller with autonomous wind disturbance recognition in free flight. However, these methods either require higher payload and power to be able to use on a FWMAV with the available airflow sensor design, or require platform-dependent modeling and controller design in advance.

A simple, yet effective solution is desired for a flapping wing MAV such that it can sense the airflow onboard and use the airspeed information in real time to improve flight stability. We present a novel approach to tackle this challenge using thermistor-based airflow sensing on a FWMAV Delfly Nimble (minimal takeoff weight: 28.2g [15]) as shown in Fig. 1. The performance reliability and a thorough characterization of a commercial off-the-shelf thermistor-based airflow sensor RevP[1] is at first presented, driving the redesign phase later for a further miniaturized sensor suited for lightweight FWMAVs applications. Following the integration of the sensor onboard the Delfly Nimble, we demonstrate how airflow sensing aids flight stability under wind influences with a computationally-inexpensive gain-scheduling approach. Results show the effectiveness of the proposed redesigned sensing solution, and its applicability to improve FWMAVs flight stability in dynamic conditions.

II. Sensor Characterization

A. Working Principle

The commercial off-the-shelf RevP airflow sensor shown in Fig. 2 works as a standard constant temperature anemometer. When the electrically heated thermistor is placed in the airflow, heat transfers from the thermistor to the flow, resulting in a temperature decrease. A bridge feedback control in the circuitry acts to vary the current flowing through the sensing thermistor to retain the temperature constant. This change in the output

[1]https://moderndevice.com/product/wind-sensor-rev-p/

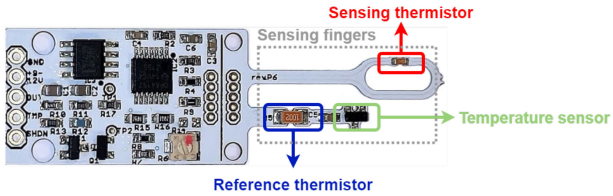

Fig. 2. RevP sensor sensing fingers' main components. This image is a photograph taken by the authors of an actual COTS product from Modern Device. Minor version changes in design depend on the purchased source and time.

current becomes a measure of flow speed change, in the form of output voltage [16]. The choice of the thermistors and power consumption restrictions from a certain MAV platform affect the design of operating voltage, measurement range, and overall performance of such an airflow sensor.

B. Calibration for Low Airflow Speeds

To acquire sufficient measurement accuracy at low airflow speeds, calibrating the airflow sensor is necessary before any further application. To perform this low-speed calibration, a reliable reference source such as an air velocity calibrator (TSI Model 1127[2]) commonly used for hot-wire calibration is used. This device is connected to pressurized air supply. Air travels through a settling chamber and emerges through an exit nozzle, where the airflow sensor's sensing fingers are placed 4 mm above the nozzle. To control the actual exit flow velocity accurately, the calibrator is equipped with two rotating knobs: a coarse one for reaching the approximate airflow speed, and a delicate one for fine adjustments. With the secondary nozzle set No.3 equipped, the calibrator is able to calibrate for flow speeds between 0.1 to 5 m/s, with a reliable resolution of 0.1 m/s. Such a secondary nozzle is much smaller in diameter compared to the exit nozzle. This leads to a low speed free jet with a differential pressure still large enough to be measured accurately with an external pressure transducer (Mensor DPG 2100). By relating this differential pressure Δp to the control velocity V through the secondary nozzle with the isentropic relations shown in (1) to (4)[3], the actual flow speed reaching the airflow sensor can then be calculated with a 9^{th}-order polynomial provided by the TSI user manual.

$$a_0 = \sqrt{\gamma\, R\, (T + 273.15)} \tag{1}$$

$$M = \sqrt{2\frac{\left(\frac{P+\Delta p}{P}\right)^{\frac{\gamma-1}{\gamma}} - 1}{\gamma - 1}} \tag{2}$$

$$a = \sqrt{\frac{a_o^2}{1 + \left(\frac{\gamma-1}{2} M^2\right)}} \tag{3}$$

$$V = M \cdot a \tag{4}$$

As the flow temperature variation in the indoor testing environment is negligibly small, the analog voltage signal from the

[2]https://tsi.com/product-accessories/manual-velocity-calibrator-without-pressure-transducer-1127/

[3]a: speed of sound [ms]; γ: specific heat ratio [-]; R: universal gas constant [J (K mol); T: temperature [°C]; M: Mach number; P: pressure [Pa]

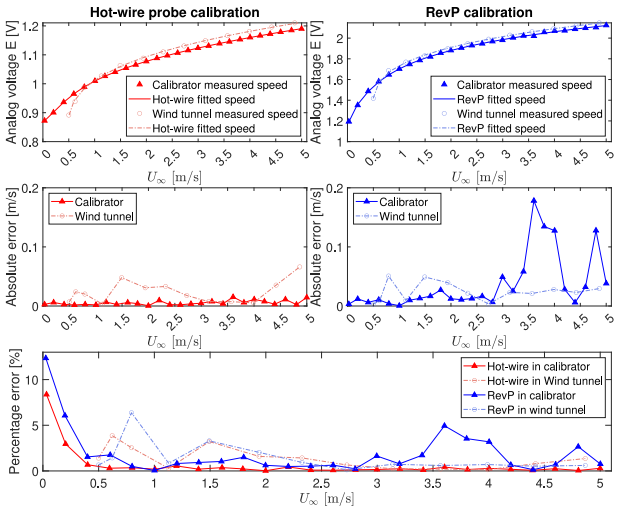

Fig. 3. Hot-wire probe and RevP airflow sensor calibrated in the calibrator device and in the wind tunnel using King's Law. The King's Law coefficients are shown in Table IV.

airflow sensor is considered as a function of only flow velocity, expressed in King's Law shown in (5), which is conventionally used in hot-wire calibration [11]. To obtain the King's Law coefficients, RevP's analog outputs E at various flow speeds are correlated with reference flow speeds V from the calibrator device through a normal least squares fit to a fourth-order polynomial shown in (6), expanded from King's Law, where U is the fitted speed. Data are sampled at 5KHz for 5 seconds at each flow speed using National Instrument DAQ NI9215, before being time-averaged and curve fitted. A reference calibration using the TU Delft low speed wind tunnel and a 5 μm tungsten hot-wire probe (interfaced with a DANTEC MiniCTA system) is also performed to compare with the calibrator's quality. Results are shown in Fig. 3. Overall, the same calibration technique using different reference flow for both sensing instrumentation has a good agreement, with an absolute error less than 0.1 m/s for most tests, and a percentage error less than 2% (0.65%, 1.36%, 1.91%, 1.45% averaged from the four cases presented in Fig. 3 final subplot), although the calibrator device has the advantage of more accessible lab use and better resolution at low flow speeds where the wind tunnel's operational range has been pushed to the limit.

$$E^2 = A + BU^n; \;\; n = 0.5 \tag{5}$$

$$U(E) = P_4E^4 + P_3E^3 + P_2E^2 + P_1E + P_0 \tag{6}$$

C. Directional Sensitivity

In order to investigate the airflow sensor's directional dependence, measurements need to be performed when the airflow sensor's sensing fingers face the incoming freestream at various incidence angles. To achieve the three rotational degrees of freedom, two stepper motors are installed as rotational mechanisms to the sensor's holder in the wind tunnel and are programmed to rotate the airflow sensor for 360 degrees at a step size of about five degrees (4.946 to be more accurate). Data

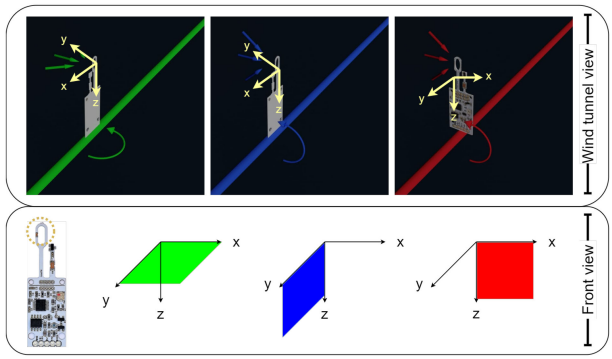

Fig. 4. Illustration of the planes of rotation to investigate the airflow sensor's directional dependence.

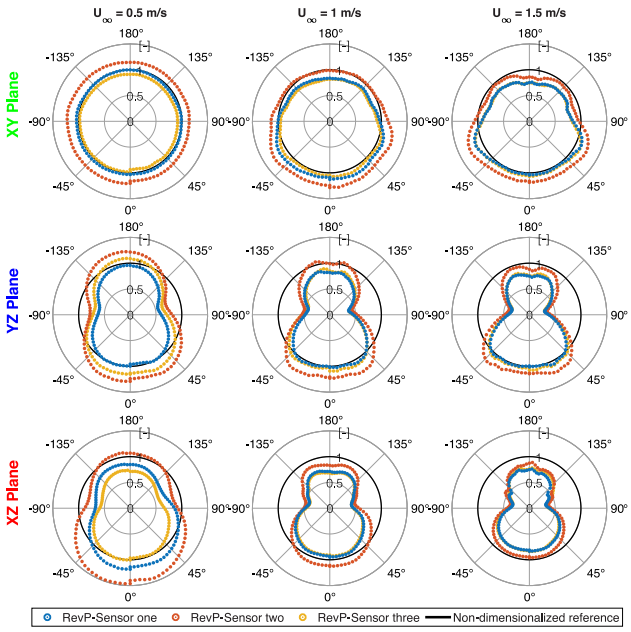

Fig. 5. RevP directional sensitivity in XY, YZ, and XZ plane at different freestream speeds.

is sampled at 5000 Hz for five seconds at each step to allow enough settling time before the sensor is in motion again. The rotational tests are repeated for three RevP sensors using the same calibration coefficients acquired from the calibrator device.

The planes of rotation XY, YZ, and XZ are defined in Fig. 4, with the sensing thermistor of the airflow sensor as the point of origin. When the front side of the sensing fingers face the incoming flow directly, the full contact between the thermistor surface and the airflow enables more sufficient heat transfer such that an optimal measurement of the true airflow speed is achieved, as reflected through the XY plane plots in Fig. 5. Despite being carefully tuned using a potentiometer onboard the RevP sensor by the manufacturer, small deviations between the sensors could account for more than 0.1 m/s difference in measurements.

These rotational tests also suggest that the RevP's measurement is directionally independent for incoming airflow as long as the incidence angle is within approximately ± 45 degrees in

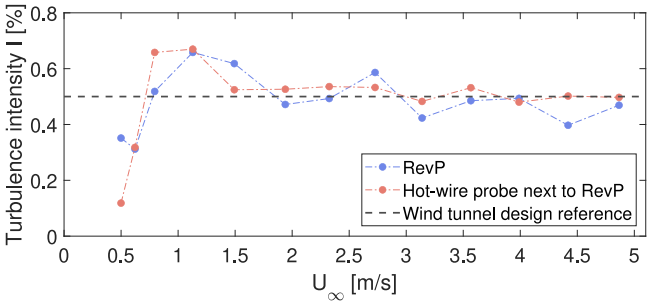

Fig. 6. Turbulence intensity from hot-wire and RevP measurements in W-tunnel 40 cm × 40 cm test section, hot-wire probe placed 5 cm apart from the RevP sensor. Sample near 1 m/s is a measurement outlier, potentially due to external environment disturbance.

all directions. Beyond this range, the measurement results start to deviate from the true airflow speed and reaches the worst case when the incoming flow is tangent to the sensing fingers. This indicates that if the RevP airflow sensor is placed aligned with the lateral direction of the flapping wing MAV, then it is more suited to measure wind disturbances initiated in the longitudinal direction.

D. Comparison With a Hot-Wire Probe

To further evaluate the measurement performance in terms of turbulence intensity and frequency response of the RevP airflow sensor, a conventional hot-wire anemometer is the optimal and accessible laboratory instrument. The versatile and cost-effective DANTEC MiniCTA system used previously during calibration is used here again with a 5 μm tungsten hot-wire probe for constant temperature anemometry. The raw analog voltage signal is sampled at 5000 Hz for five seconds at each flow speed. The flow turbulence intensity I is calculated based on (7), which leads to the results shown in Fig. 6. The close alignment between the two instruments demonstrates a comparable measurement capacity and accuracy for fluctuations, as the Wind tunnel is designed to have minimum achievable turbulence intensity level at the order of 0.5% when producing laminar flow, which is reflected in the measurement results.

$$I = \frac{u_{RMS}}{\bar{u}} = \frac{\sqrt{\frac{1}{N}\sum_{i=1}^{N}(u_i - \bar{u})^2}}{\bar{u}} \tag{7}$$

When the wind tunnel's flow turbulence level is increased by an add-on grid of porosity 56.25%, flow measurements are taken at 20 cm downstream of the add-on grid. Spectral analysis with power spectral density is performed on the raw output voltage signals from both the RevP and the hot-wire measurements. As shown in Fig. 7, the energy level of the different frequency components for RevP reaches a noise floor approximately 30, 200, and 400 Hz earlier than the hot-wire probe at the three freestream speeds, indicating a sufficient yet worse performed frequency response.

E. Characterization Results

The detailed calibration results show ease of calibration of the RevP sensor at the low speed range, when given the availability

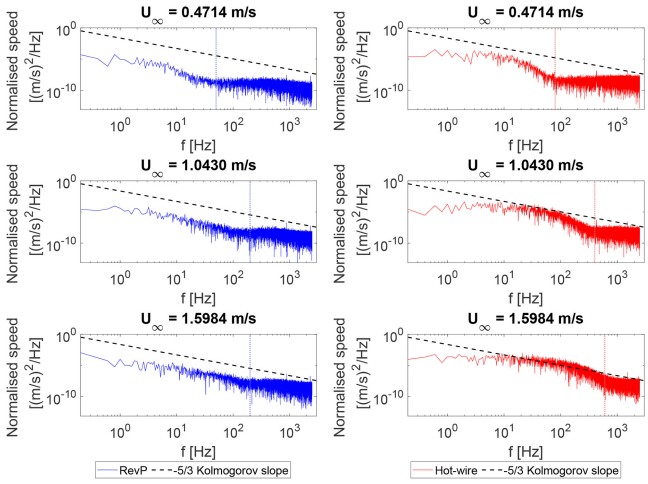

Fig. 7. Power spectral density and frequency log-log plot of RevP and hot-wire measurements at different freestream speeds, with an add-on grid for increased flow disturbance; the -53 Kolmogorov slope displayed as reference.

of a good reference flow source. The low speed measurement has a good resolution till within 0.5 m/s, as also reported by Prohasky *et al.* [17]. In terms of directional sensitivity, the RevP sensor provides reliable one-directional flow measurement within ± 45 degrees with respect to the incoming airflow. Further performance analysis shows that the RevP sensor has sufficient frequency response to measure flow fluctuations for low speed applications. For future applications, the temperature dependent effects of the sensor at various test environment temperatures could be studied to deepen the analysis of measurement accuracy and enlarge the sensor's operational temperature ranges.

III. Tethered Flights in the Wind Tunnel

A. Experimental Setup

Since FWMAVs generate a periodic airflow around the body due to the flapping cycle, we first investigate how much this influences the airflow sensor readings with tethered flights in a wind tunnel. The results of this intermediate test campaign also help us to evaluate the sensor's capability to differentiate between various ambient flow speeds, despite the periodic flow influence induced by the flapping motion itself. Moreover, as the pitch angle is the most significant for MAV's attitude stability when encountering perturbation [18], airflow sensing under various pitch angles is also investigated.

The custom-made test rig and the pitch-angle-adjustment mechanism to tether the Delfly Nimble for different testing configuration are shown in Fig. 8. The RevP sensor is placed on top of the Delfly Nimble fuselage (a 2 mm × 2 mm carbon rod) with a lightweight, small-size 3D-printed structure binding it tightly to the fuselage. Despite being the only rigid area on the flapping wing MAV, this placement location is also chosen based on the bio-inspiration from avian head stabilization capability to attenuate body oscillations throughout the wingbeats [19], and being ahead of the leading edge makes the airflow sensing phase-advanced [20].

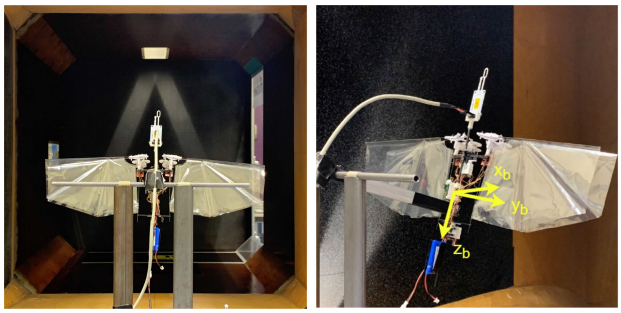

Fig. 8. Delfly tethered on a support structure for flapping tests, placed at the exit of the wind tunnel 60 × 60 [cm] section. Body frame axes x_b, y_b, z_b define roll, pitch, and yaw respectively.

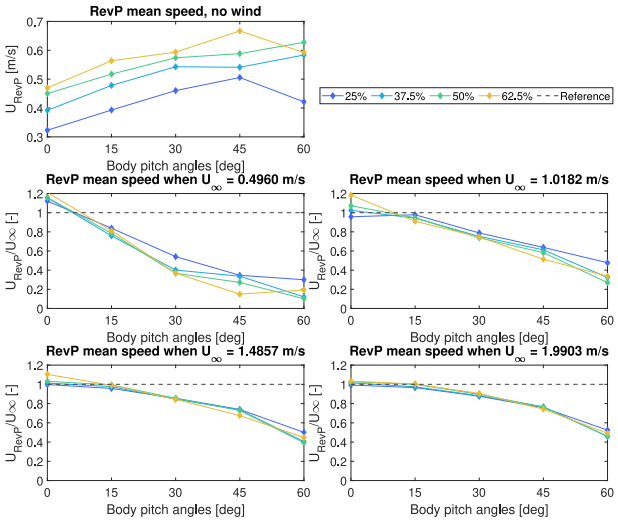

Fig. 9. Delfly Nimble with RevP sensor onboard, at various flapping frequencies controlled through various throttle levels at 25%, 37.5%, 50%, 62.5% (flapping frequency is ≈17 Hz for hovering in free-flight with 65% throttle level [15]); forward body pitch angles at 0, 15, 30, 45, and 60 degrees (absolute values are hereby for clarity, however actual pitch angles are negative w.r.t. the body frame); and ambient flow speeds approximately at 0, 0.5, 1.0, 1.5, and 2.0 m/s.

B. Results

The influence of different throttle levels, body pitch angles, and freestream speeds are shown in Fig. 9. When there is no wind disturbance, the relative movement of the RevP sensor caused by the flapping motion and the potential influence from the wake accounts for the airflow speed measurement at the magnitude of approximately 0.5 m/s, which is non-negligible considering how susceptible the vehicle is to wind disturbances. For the plots with ambient flow, the previous windless measurement values are accounted for to minimize the influence of flapping motions to the true airflow speed measurements. The results are a-dimensionalized with the respective ambient flow speeds. It can be seen that the RevP sensor is capable of measuring the ambient flow speed more accurately for smaller body pitch angles less than 15 degrees, and at higher ambient flow speeds where low-speed measurement noise is less significant. The RevP sensor's directional sensitivity also comes into play as the angle between the incoming flow and the sensing thermistor

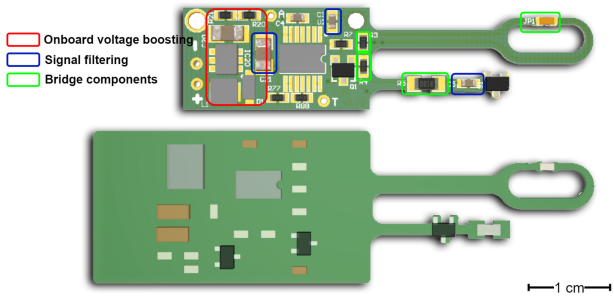

Fig. 10. Schematic illustration of the redesigned airflow sensor and size comparison with the commercial version. New components consist of DC-DC power converter marked in red, modified components marked in blue and green.

TABLE I
REVP AIRFLOW SENSOR KEY SPECIFICATIONS BEFORE AND AFTER THE REDESIGN

RevP	Mass [g]	Supply voltage [V]	Current [A]
Original	1.34	12	0.03-0.04**
New	0.76	3.9-4.1*	0.05-0.08**

*with a DC-DC converter.
**current drawn under airflow speeds from 0-5 m/s.

increases with an increase in body pitch angle. As the RevP sensor's directional dependence deteriorates rapidly beyond ±45 degrees, the measured airflow speed drops to 20-40% of the reference freestream speeds.

IV. Free-Flight Experiments Under Wind Disturbances

A. Redesign of the RevP Airflow Sensor

To implement the onboard airflow sensing capability on the flapping wing robot Delfly Nimble, the RevP airflow sensor with 1.34 g mass, 12 V supply voltage, and up to 0.04 A current consumption is not fully suited. To accommodate for the right voltage supply, a voltage converter would be needed on the original sensor, bringing a higher toll on payload and flight time. In virtue of this, a redesigned smaller printed circuit board (PCB) with an integrated DC-DC converter is proposed to meet our platform's requirements, see Fig. 10. The newly-fitted voltage converter is made of a Schottky diode (0.5 A, 30 V), an energy storage element of one 4.7 μH inductor and one 4.7 μF capacitor, a MCP1661T-E/OT MICROCHIP voltage regulator, and an extra 10 μF capacitor for more stable boosted voltage.

After the redesign and fabrication, the new airflow sensor is over 40% lighter and about 55% smaller with the key specifications shown in Table I. With the integration of the new sensor on the Delfly Nimble, the total take-off weight is reduced by 0.8 g, totalling 30.5 g. The same calibration procedure using the air velocity calibrator described in Section II is applied to the redesigned RevP sensor to acquire the new voltage-speed relationship before the free flight experiments in wind conditions.

B. Experimental Setup

To perform repeatable flight tests under wind disturbances, guided position control is utilized as illustrated in Fig. 11. Delfly

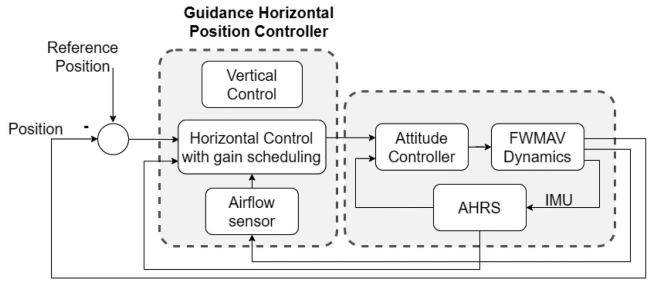

Fig. 11. Block diagram showing the implemented gain scheduling in the horizontal position controller.

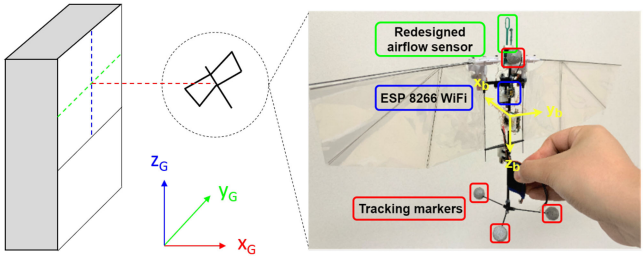

Fig. 12. Delfly Nimble hovering at the fixed waypoint in front of the fan system, with add-on hardware configuration illustrated. Reflective markers and a WiFi module are used for OptiTrack motion capture system to enable the guided position control. The global frame for position tracking originates at the fixed waypoint for hovering.

Nimble hovers at a set waypoint (1 m downstream from the fan system, with the roll axis x_b pointing towards the center of the fan system as illustrated in Fig. 12) in front of a custom-made fan system [21] that is capable of generating wind disturbances at various speeds and time duration.

The OptiTrack motion capture system provides position inputs such that the vertical and horizontal guidance control loop of the Delfly Nimble can regulate the MAV's position. The flight test set-up is shown in Fig. 12. The PD gains of the horizontal guidance position control loop are the most susceptible to wind disturbances due to the inertial force impact from the airflow in the longitudinal direction of the FWMAV and need to be tuned based on the actual airflow speeds. A set of pre-tuned gains is acquired for wind speeds approximately from 0.5 to 1.1 m/s at a step increase of 0.2 m/s, by adjusting the fan system PWM duty cycle from 20% to 35% at a step increase of 5%. Along with the stable hovering flight without any wind disturbance, these five tuning tests provide the airspeed intervals that will later be used in the gain scheduling to switch to the right set of gains suited for specific disturbance intensity. To generate repeatable wind disturbance of different intensities, the fan system PWM duty cycle is programmed to gradually increase from 0%, 20%, 25%, 30%, to 35%, and stay at each intensity for 10 seconds.

With the gain scheduling adaptive control scheme, the real-time airspeed measured by the redesigned RevP sensor will determine the actual gains used for horizontal guidance control and thus aim to keep the FWMAV stable at the desired position regardless of the wind disturbance changes. To highlight the position control improvement, extra two groups of flight tests without airflow sensor enabled gain scheduling are performed, with the first group using only the lowest gain from the list of scheduled gains, and the second group using only the highest. Each group of tests is repeated three times. The actual gains used in the three groups of tests are summarized in Table II.

TABLE II
PD GAINS USED IN THE HORIZONTAL POSITION CONTROLLER FOR FLIGHT TESTS WITH AND WITHOUT THE GAIN SCHEDULING (GS)

PD gains		K_p	K_d
With GS	PWM 0%	1100	450
	PWM 20%	1200	500
	PWM 25%	1600	490
	PWM 30%	1650	550
	PWM 35%	1700	550
No GS, low gain		1100	450
No GS, high gain		1700	550

TABLE III
COMPARISON OF RMS POSITION ERRORS WITH/WITHOUT GAIN SCHEDULING (GS) IN THE HORIZONTAL POSITION CONTROLLER

Horizontal position controller	RMS errors [cm]		
	X	Y	Z
With GS			
Test 1	19.1	4.6	10.8
Test 2	18.9	3.8	8.0
Test 3	25.3	4.5	13.9
No GS, low gain			
Test 1	25.9	6.7	6.8
Test 2	23.0	5.0	11.0
Test 3	33.8	10.2	13.1
No GS, high gain			
Test 1	17.8	4.3	23.0
Test 2	16.7	4.5	61.6
Test 3	13.7	5.3	32.0

C. Results

The repeated free-flight tests under the multiple stages of wind disturbance increase are shown in Fig. 13 with the global position deviation from the waypoint and the body pitch angle measurement. With the help of the onboard airflow sensing enabled gain scheduling for horizontal position control, Delfly Nimble is able to maintain the closest to the desired position with the best pitch stability under wind of different disturbance intensities. The low gain case leads to the FWMAV being pushed further down to the freestream. Although the high gain case is best at keeping close to the set waypoint horizontally, but at the cost of high pitch instability and large altitude fluctuations under the rapid thrust vector oscillations, which also leads to faster power depletion. This is also reflected through the position root-mean-square (RMS) error shown in Table III. Note that as the wind intensity increases, the FWMAV switches from vertical hovering position to gradually pitch forward more (from about 0 to -30 degrees) to generate enough lift to counteract the increasing wind inertial force.

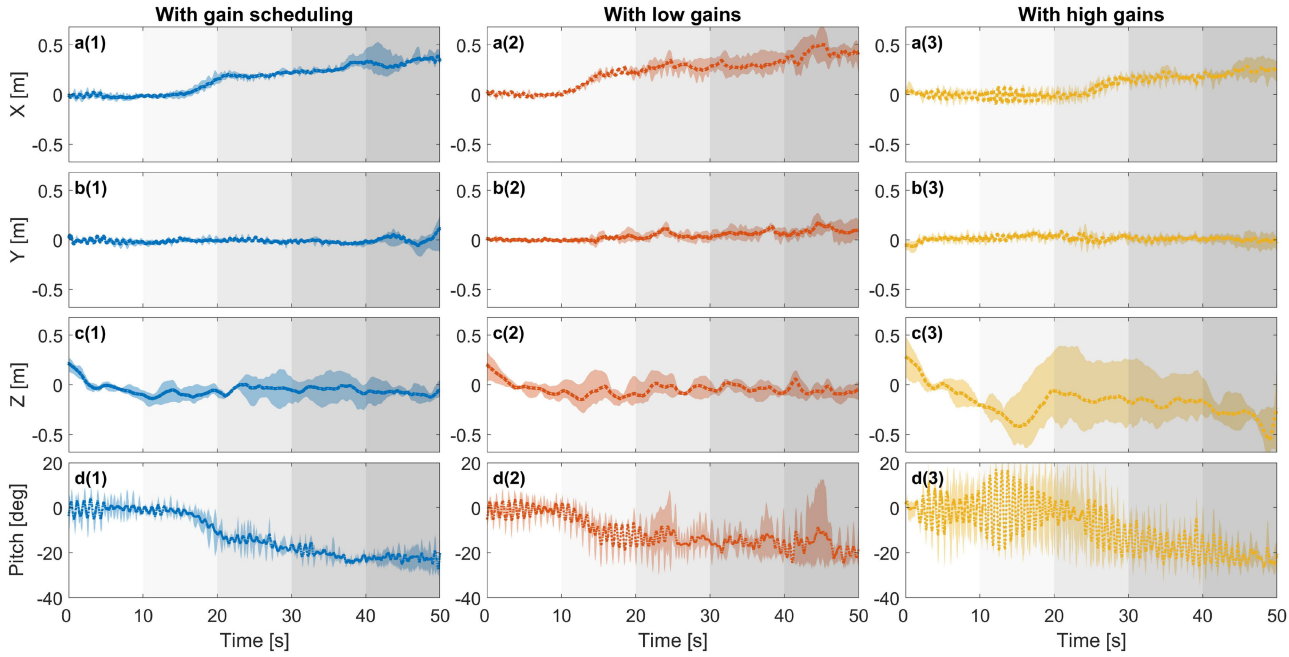

Fig. 13. Delfly Nimble hovering at or near the waypoint under different freestream speeds with or without using the gain scheduling scheme. a(1) - c(3) Position error with respect to the fixed waypoint in the global frame. The zero point indicates the set waypoint position. d(1) - d(3) Body pitch angle variations with the zero point being the vertical hovering position. Each plot is shaded with three repeated free-flight tests and the averaged value is shown in the dotted line. The gray color gradient indicates the five stages of fan system flow speeds with measurement plotted in Fig. 14.

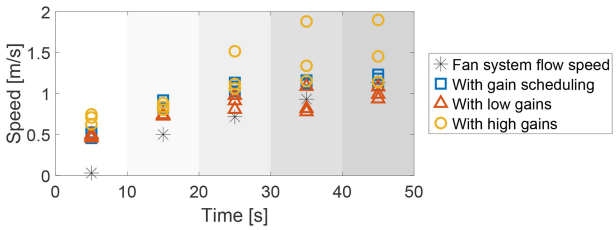

Fig. 14. Time-averaged airspeed measurement from the onboard airflow sensor at different stages of free flights under various freestream disturbance levels, compared with the freestream speeds of the fan system flow.

The time-averaged airspeed measurement at each stage of wind intensity from the three groups of tests are shown in Fig. 14, along with the freestream speed at 1 m downstream from the fan arrays as reference [21]. It can be seen that the redesigned airflow sensor is capable of providing repeatable airspeed measurement under various wind intensities overall. Only the group of tests with high gains exhibit larger airspeed fluctuations, which is a direct result of the large altitude changes as can be seen in Fig. 13 c(3). The difference between the onboard airspeed measurement and the actual freestream speed is subject to the flapping induced flow influence, as also discovered during the tethered wind tunnel tests shown in Fig. 9. As the pitch angle is dynamically changing in free-flight tests, especially at a higher magnitude for larger freestream disturbance, the directional sensitivity of the airflow sensor leads to a slight decrease in true airspeed measurement despite the flapping induced influence, as the incidence angle between the freestream and the sensing thermistor enlarges. To mitigate this insufficient measurement due to the directional dependence, the choice of the sensing thermistor and the sensing finger geometrical configuration could be improved for more uniform angular response and heat transfer surface contact in the future.

V. Conclusion

Multiple factors raise challenges to implement embodied airflow sensing on lightweight FWMAVs. At the low-flow speed regime in which FWMAVs are operable, accurate flow measurement is crucial to control robust and stable flight. To obtain adequate airflow measurement accuracy, one needs to extrapolate the influence of 1) changes in the flapping frequency, 2) cyclic changes in airflow and 3) vibrations induced by the flapping motion itself. Lastly, the airflow sensor's directional dependency affects the measurement of the true airflow speed as the FWMAV undergoes attitude changes - primarily pitch angle - due to wind disturbance. Together, these factors contribute to the complexity of working with such bio-inspired lightweight robotic platforms.

In this work, we tackle these challenges by presenting an extensive and comprehensive analysis of embodied airflow sensing on a 28.2 g flapping wing MAV, and further implement a control strategy to enable stable free-flight of such lightweight platform in different wind conditions.

After a detailed study on a commercially available sensing solution, a custom-made miniaturised 0.76 g airflow sensor is successfully integrated onboard the FWMAV. The high measurement sensitivity at extremely low flow speeds, and good resolution at the magnitude of 0.1 m/s give the flapping wing platform the capability to detect wind disturbance in real-time,

and actively change its attitude (pitch angle) for more stable flight. This allows the FWMAV to, not only endure wind disturbances up to almost 1.2 m/s with the airspeed-enabled gain scheduling for the horizontal position controller, but also to reach better positioning accuracy and thrust management.

Future work will investigate the possibility to extend the thermistor-based sensing capabilities in terms of size, shape, measurement range, heat dissipation and onboard temperature regulation for broader applications. With its small form factor and easy onboard integration, this work opens the scope to further improvements of in-gust flight performance using a combined strategy of mechanical augmentation [22], embodied airflow sensing and active control methods.

APPENDIX

TABLE IV
REVP SENSOR KING'S LAW CALIBRATION COEFFICIENTS AT ROOM TEMPERATURE (20 °C), WITH DIFFERENT CALIBRATION TOOLS

	P_4	P_3	P_2	P_1	P_0
Calibrator	8.4080	-46.2862	97.5318	-91.6633	32.1309
W-tunnel	4.5646	-22.2505	42.5811	-38.4583	14.3975

ACKNOWLEDGMENT

We would like to thank Paul Badger, the "Inventor" of the original RevP sensor from Modern Device, for providing useful documentation that helped with the further customization of the sensor; TU Delft Low Speed Lab engineer Stefan Bernardi for helping setting up the calibration and wind tunnel experiments. We would also like to thank Dr. Marios Kotsonis, PhD candidate Edoardo Saredi, and start-up company Dimple Technology for their help on the hot-wire instrumentation; and Martijn den Hoed for assisting in flight preparation and testing.

REFERENCES

[1] J. Sundin, K. Kokmanian, M. K. Fu, S. Bagheri, and M. Hultmark, "A soft material flow sensor for micro air vehicles," *Soft Robot.*, vol. 8, no. 2, pp. 119–127, 2021.

[2] Y. Ozaki, T. Ohyama, T. Yasuda, and I. Shimoyama, "An air flow sensor modeled on wind receptor hairs of insects," in *Proc. IEEE 13th Annu. Int. Conf. Micro Electro Mech. Syst.*, 2000, pp. 531–536.

[3] M. Dijkstra, J. Van Baar, R. J. Wiegerink, T. S. Lammerink, J. De Boer, and G. J. Krijnen, "Artificial sensory hairs based on the flow sensitive receptor hairs of crickets," *J. Micromechanics Microeng.*, vol. 15, no. 7, 2005, Art. no. S132.

[4] J. Casas, T. Steinmann, and G. Krijnen, "Why do insects have such a high density of flow-sensing hairs? Insights from the hydromechanics of biomimetic MEMS sensors," *J. Roy. Soc. Interface*, vol. 7, no. 51, pp. 1487–1495, 2010.

[5] H. Takahashi, E. Iwase, K. Matsumoto, and I. Shimoyama, "Air flow senser for an insect-like flapping wing," in *Proc. IEEE 21st Int. Conf. Micro Electro Mech. Syst.*, 2008, pp. 916–919.

[6] K. Najafi, "Biomimetic hair sensors: Utilizing the third dimension," in *Proc. IEEE SENSORS*, pp. 1–4, 2012.

[7] S. D. Gollob, Y. Manian, R. S. Pierre, A. S. Chen, and S. Bergbreiter, "A lightweight, compliant, contact-resistance-based airflow sensor for quadcopter ground effect sensing," in *Proc. IEEE Int. Conf. Robot. Automat.*, 2018, pp. 7826–7831.

[8] H.-S. Shin, T. Kim, S. Bergbreiter, and Y.-L. Park, "Biomimetic soft airflow sensor with printed ionogel conductor," in *Proc. IEEE 2nd Int. Conf. Soft Robot.*, 2019, pp. 611–616.

[9] K. Rajasekaran, H. D. Bae, S. Bergbreiter, and M. Yu, "3D printed bio-inspired hair sensor for directional airflow sensing," in *Proc. IEEE/RSJ Int. Conf. Intell. Robots Syst.*, 2020, pp. 8945–8950.

[10] A. Dijkshoorn, J. Cui, S. Stramigioli, and G. Krijnen, "First results of a soft, 3D-printed, resistive cantilever flow sensor," in *Proc. IEEE Int. Conf. Flexible Printable Sensors Syst.*, 2021, pp. 1–4.

[11] J. Keshavan and J. S. Humbert, "MAV stability augmentation using weighted outputs from distributed hair sensor arrays," in *Proc. Amer. Control Conf.*, 2010, pp. 4445–4450.

[12] B. N. Ranganathan, I. Penskiy, W. Dean, S. Bergbreiter, and J. S. Humbert, "Bio-inspired wind frame state sensing and estimation for MAV applications," in *Proc. IEEE/RSJ Int. Conf. Intell. Robots Syst.*, 2015, pp. 2729–2735.

[13] P. Chirarattananon, Y. Chen, E. F. Helbling, K. Y. Ma, R. Cheng, and R. J. Wood, "Dynamics and flight control of a flapping-wing robotic insect in the presence of wind gusts," *Interface Focus*, vol. 7, no. 1, 2017, Art. no. 20160080.

[14] J. Lee, S. Ryu, and H. J. Kim, "Stable flight of a flapping-wing micro air vehicle under wind disturbance," *IEEE Robot. Automat. Lett.*, vol. 5, no. 4, pp. 5685–5692, Oct. 2020.

[15] M. Karásek, F. T. Muijres, C. De Wagter, B. D. Remes, and G. C. De Croon, "A tailless aerial robotic flapper reveals that flies use torque coupling in rapid banked turns," *Science*, vol. 361, no. 6407, pp. 1089–1094, 2018.

[16] H. Bruun, *Hot-Wire Anemometry: Principles and Signal Analysis*. Oxford, U.K.: Oxford Univ. Press, 1995.

[17] D. Prohasky and S. Watkins, "Low cost hot-element anemometry verses the TFI Cobra," in *Proc. 19th Australas. Fluid Mechanics Conf.*, 2014, pp. 1–4.

[18] M. Thompson, S. Watkins, C. White, and J. Holmes, "Span-wise wind fluctuations in open terrain as applicable to small flying craft," *Aeronautical J.*, vol. 115, no. 1173, pp. 693–701, 2011.

[19] A. E. Pete, D. Kress, M. A. Dimitrov, and D. Lentink, "The role of passive avian head stabilization in flapping flight," *J. Roy. Soc. Interface*, vol. 12, no. 110, 2015, Art. no. 20150508.

[20] A. Mohamed, S. Watkins, R. Clothier, M. Abdulrahim, K. Massey, and R. Sabatini, "Fixed-wing MAV attitude stability in atmospheric turbulence—Part II: Investigating biologically-inspired sensors," *Prog. Aerosp. Sci.*, vol. 71, pp. 1–13, 2014.

[21] D. A. Olejnik *et al.*, "An experimental study of wind resistance and power consumption in MAVs with a low-speed multi-fan wind system," in *Proc. IEEE Int. Conf. Robot. Automat.*, 2022, pp. 2989–2994.

[22] D. A. Olejnik, F. T. Muijres, M. Karásek, L. H. Camilo, C. De Wagter, and G. C. de Croon, "Flying into the wind: Insects and bio-inspired micro-air-vehicles with a wing-stroke dihedral steer passively into wind-gusts," *Front. Robot. AI*, vol. 9, 2022, Art. no. 820363.